White Rose Research Online

eprints@whiterose.ac.uk
https://eprints.whiterose.ac.uk
Universities of Leeds, Sheffield and York

Deposited via The University of Leeds.

White Rose Research Online URL for this paper:
https://eprints.whiterose.ac.uk/id/eprint/151775/

Version: Accepted Version

Article:
Arribas Perez, M, Moriones, OH, Bastús, NG et al. (2019) Mechanomodulation of Lipid Membranes by Weakly Aggregating Silver Nanoparticles. Biochemistry, 58 (47). pp. 4761-4773. ISSN: 0006-2960

https://doi.org/10.1021/acs.biochem.9b00390

Reuse
Items deposited in White Rose Research Online are protected by copyright, with all rights reserved unless indicated otherwise. They may be downloaded and/or printed for private study, or other acts as permitted by national copyright laws. The publisher or other rights holders may allow further reproduction and re-use of the full text version. This is indicated by the licence information on the White Rose Research Online record for the item.

Takedown
If you consider content in White Rose Research Online to be in breach of UK law, please notify us by emailing eprints@whiterose.ac.uk including the URL of the record and the reason for the withdrawal request.

UNIVERSITY OF LEEDS
University of Sheffield
UNIVERSITY of York

Mechanomodulation of lipid membranes by weakly aggregating silver nanoparticles

Marcos Arribas Perez[1,2], Oscar H. Moriones[3,4], Neus G. Bastús[3], Victor Puntes[3,4,5,6], Andrew Nelson[1] and Paul A. Beales[1,2,*]

1. *School of Chemistry, University of Leeds, Leeds, LS2 9JT, UK.*
2. *Astbury Centre for Structural Molecular Biology, University of Leeds, Leeds, LS2 9JT, UK.*
3. *Institut Català de Nanociència y Nanotecnologia (ICN2),Campus UAB,08193, Bellaterra, Barcelona, Spain.*
4. *Universitat Autonòma de Barcelona (UAB), campus UAB, 08193, Bellaterra, Barcelona, Spain.*
5. *Vall d`Hebron Institut de Recerca (VHIR), 08035, Barcelona, Spain.*
6. *Institució Catalana de Recerca i Estudis Avançats (ICREA), 08010, Barcelona, Spain.*

* Corresponding author: p.a.beales@leeds.ac.uk

Keywords: Nanotoxicology, colloidal stability, medium effects, mechanobiology, lipid bilayer, vesicles

ABSTRACT

Silver nanoparticles (AgNPs) have wide-ranging applications, including as additives in consumer products and in medical diagnostics and therapy. Therefore understanding how AgNPs interact with biological systems is important for ascertaining any potential health risks due to the likelihood of high levels of human exposure. Besides any severe, acute effects, it is desirable to understand more subtle interactions that could lead to milder, chronic health impacts. Nanoparticles are small enough to be able to enter biological cells and interfere with their internal biochemistry. The initial contact between nanoparticle and cell is at the plasma membrane. To gain fundamental mechanistic insight into AgNP-membrane interactions, we investigate these phenomena in minimal model systems using a wide-range of biophysical approaches applied to lipid vesicles. We find a strong dependence on the medium composition, where colloidally stable AgNPs in a glucose buffer have negligible effect on the membrane. However, at a physiological salt concentrations, the AgNPs start to weakly aggregate and sporadic but significant membrane perturbation events are observed. Under these latter conditions, transient poration and structural remodelling of some vesicle membranes is observed. We observe that the fluidity of giant vesicle membranes universally decreases by an average of 16% across all vesicles. However, we observe a small population of vesicles display a significant change in mechanical properties with lower bending rigidity and higher membrane tension. Therefore we argue that the isolated occurrences of membrane perturbation by AgNPs are due to low probability mechanomodulation by AgNP aggregation at the membrane.

GRAPHICAL ABSTRACT

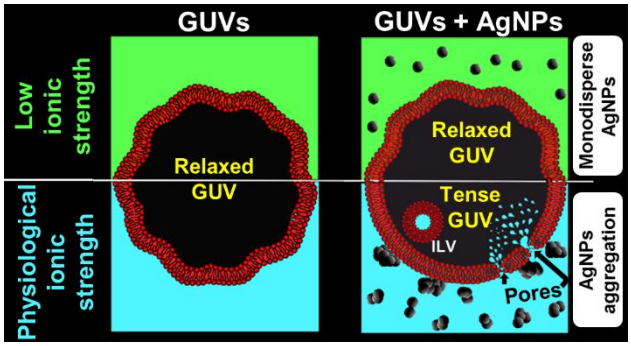

INTRODUCTION

Engineered nanomaterials or nanoparticles (NPs) have a very high surface-to-volume ratio that modifies their physicochemical properties due to being largely composed of high energy surface atoms compared to atoms existing in the more stable "bulk" [1]. These novel properties affect the biological activity and biocompatibility of NPs and can lead to advantageous characteristics for their application in biomedicine as therapeutic and diagnosis systems [2, 3]. To perform the desired biomedical function, NPs often must be able to pass across lipid biomembranes to reach specific subcellular targets. However, this NP translocation may result in undesirable membrane perturbations and dysregulation of biochemical processes which can lead to severe cell damage and even cell death [4-7].

Noble metal NPs, especially silver nanoparticles (AgNPs), are the most widely used nanomaterials[8, 9]. Due to their unique electrical, thermal, optical, antibacterial and anti-inflammatory properties, AgNPs have been largely studied for biomedical applications, such as biosensing, imaging, diagnosis, and antimicrobial therapies[10, 11]. Additionally, AgNPs have been proposed as a potential candidate for cancer theranostics, which allows the simultaneous accurate diagnosis and targeted treatment of the disease [12]. Despite all these advantageous properties, AgNPs have been reported to occasionally cause serious injuries to eukaryotic cells, but the mechanisms behind this cytotoxicity are still not well understood [13]. In this context, the interaction of AgNPs with the membrane is essential for their biomedical activity but is also the initial step of the toxicity pathway. This interaction often lead to the internalisation of the NPs by the membrane and can induce loss of membrane integrity [14, 15]. Once internalised, AgNPs could cross and damage other sub-cellular membranes to enter important organelles, such as mitochondria, and originate endogenous reactive oxygen species (ROS) [14-16]. Endogenous ROS are mainly generated by the dysregulation of the respiratory chain of the inner mitochondrial membrane [17]. While the

toxicity of AgNPs is currently primarily attributed to the release of soluble silver ions[18, 19], it is plausible that the increase of endogenous ROS is, at least in part, related with the ability of AgNPs to disrupt lipid membranes [19]. However, corrosion processes are also REDOX active and induces ROS [20], especially in chemically labile NPs, such as AgNPs.

NP-membrane interactions are extremely complex processes and involve several attractive and repulsive forces acting together at the nanoparticle-membrane interface (nanobio interface) [21]. The nature of the NP-biomembrane interactions and their potential toxicity do not only depend on the composition of the NPs, but are also determined by numerous physicochemical properties of NPs. The size and shape of NPs play a significant role in the interaction mechanism of nanomaterials with biological membranes. Zhang *et al* showed that 18 nm SiO_2 NPs cause permanent holes in giant unilamellar vesicles (GUVs) and a decrease in lipid lateral diffusion, whereas SiO_2 NPs larger than 78 nm are wrapped by the membrane and lead to an increase in membrane fluidity [22]. Chithrani *et al* observed higher cellular uptake of spherical gold NPs (AuNPs) into HeLa cells than rod-shaped AuNPs [23]. Additionally, NP-biomembrane interactions are highly dependent on surface modifications and the charge of NPs. Moghadam *et al* modified the surface coating and charge of AuNPs and titanium dioxide (TiO_2) NPs and observed that AuNPs and TiO_2 NPs with positive charge significantly increase the permeability of DOPC membranes while the dye leakage caused by negatively charged NPs is insignificant [24]. A similar behaviour has been recently reported by Montis *et al* who showed that cationic AuNPs induce more drastic effects on zwitterionic and negatively charged membranes than anionic and PEG-coated AuNPs [25]. Moreover, the properties of the surrounding medium, such as pH, temperature, ionic strength, macromolecular crowding, and viscosity can modify many important characteristics of NPs such as surface charge, solubility and colloidal stability, and also can modulate their biological activity [21, 26, 27]. The considerably large number of parameters

98 influencing the NP behaviour along with the complexity of biological membranes, makes the
99 understanding of NP-membrane interactions very challenging.

100 The high complexity of the system represent a limitation for understanding specific
101 mechanisms behind the interaction between NPs and cell membranes. To deal with this
102 issue, it is fundamental to find ways to reconstitute simpler *in vitro* model systems that are
103 easier to control and systematically investigate. One example of such *in vitro* systems are
104 biomimetic model membranes which are synthetic lipid bilayers where the lipid composition
105 can be selected, the lipids can be modified, for example labelled with a fluorescent dye, the
106 number of biomolecular components can be reduced and the medium conditions can be
107 tightly controlled [28, 29]. These artificial model membranes can be investigated using a
108 multitude of biophysical techniques, including calorimetry, spectroscopy and microscopy.
109 This provides detailed information on the structure, mechanics, dynamics and functions of
110 model membranes as well as on their interactions with matter in their local environment, in
111 this case engineered nanoparticles.

112 In this investigation, we use advanced spectroscopy and microscopy techniques to
113 study changes in the physicochemical properties of lipid membranes upon interaction with
114 AgNPs. Our experiments are performed on large unilamellar vesicles (LUVs) and GUVs.
115 Ensemble characterisation of LUVs (400 nm diameter) provides valuable information about
116 the average behaviour of the vesicles in the sample, whereas GUVs are cell-sized model
117 membranes which are observable by optical microscopy at the single vesicle level and
118 hence allow us to detect rare events, transient processes and study the true distribution of
119 complex behaviours in our experiments [28].

MATERIALS AND METHODS

Materials

1,2-dioleoyl-sn-glycero-3-phosphocholine (DOPC) lipid and 1,2-dioleoyl-sn-glycero-3-phosphoethanolamine-N-(lissamine rhodamine B sulfonyl) (ammonium salt) (18:1 lissamine rhodamine PE) were purchased from Avanti Polar Lipids Inc. (Alabaster, Alabama, USA). Indium tin oxide (ITO) coated glass slides (surface resistivity 8–12 V sq-1), 4-(2-hydroxyethyl)-1-piperazineethanesulfonic acid (HEPES), silver nitrate ($AgNO_3$), trisodium citrate ($Na_3C_6H_5O_7$), and tannic acid ($C_{76}H_{52}O_{46}$) sodium chloride (NaCl), glucose ($C_6H_{12}O_6$), sodium hydroxide (NaOH), and bovine serum albumin (BSA) were obtained from Sigma-Aldrich Co. (Gillingham, UK). 5(6)-carboxyfluorescein, 10 kDa dextran labelled with cascade blue, were purchased from ThermoFisher Scientific Ltd. (Loughborough, Leicestershire, UK). Microscope µ-slide 8 well glass bottom chambers (Ibidi GmbH) were purchased from Thistle Scientific Ltd (Glasgow, UK).

Buffer composition

The experiments were conducted in two different buffers with high and low ionic strength, respectively. The high ionic strength buffer (HEPES saline buffer) consists of 20 mM HEPES and 150 mM NaCl, resembling the ionic strength of physiological media. In contrast, the low ionic strength buffer (HEPES glucose buffer) also contains 20 mM HEPES but 300 mM glucose instead of salt to maintain the same osmolality of the medium in all the experiments. Both buffers were adjusted to pH 7.4 with NaOH.

Synthesis of AgNPs

Silver nanocrystals of ~20 nm in diameter were prepared by the seeded-growth method recently reported by Bastús *et al* [30]. In a typical experiment, 100 mL volume of

aqueous solution containing 5 mM of sodium citrate (SC) and 0.1 mM of tannic acid (TA) was prepared and heated up to 100°C with a heating mantle in a three-neck round bottomed flask for 15 minutes under vigorous stirring. A condenser was used to prevent the evaporation of the solvent. After boiling had commenced, 1 mL of 25 mM of $AgNO_3$ was injected into this solution. The solution became bright yellow immediately indication the formation of the Ag seeds. Immediately after the synthesis of Ag seeds and in the same vessel, the as-synthetized silver seeds were grown by cooling down the solution to 90°C. First, the seed solution was diluted by extracting 20 mL of sample and adding 17 mL of Milli-Q-water. Then 500 µL of SC [25 mM], 1.5 mL of 2.5 mM TA and 1 mL of 25 mM $AgNO_3$ were sequentially injected. This process was repeated up to 2 times, progressively growing the size of the AgNPs until reaching the size ~20 nm ($\sim 1.8\times10^{12}$ NPs/mL). The obtained AgNPs were purified by centrifugation and stored in a solution containing both TA and SC.

UV–Vis Spectroscopy

UV–visible spectra were acquired with a Shimadzu UV-2401 PC spectrophotometer. A 10% (v/v) of AgNP solution was placed in a cell and the spectral analysis was performed in the 300–800 nm wavelength range at room temperature.

Transmission Electron Microscopy

Transmission electron microscopy (TEM) images were acquired with a FEI Tecnai G2 F20 S-TWIN HR(S) TEM equipped with an energy-dispersive X-ray spectroscopy (EDX) detector, operated at an accelerated voltage of 200 kV. A 10 µL droplet of the sample was drop cast onto a piece of ultrathin carbon-coated 200-mesh copper grid (Ted-pella, Inc.) and left to dry in air. The size of more than 500 particles was computer-analysed using Image J software and measured to calculate size distributions profiles.

Dynamic light scattering (DLS)

Dynamic light scattering (DLS) and dynamic electrophoretic light scattering (DELSA) were employed to measure the hydrodynamic diameter and the ζ potential of AgNPs, respectively, using a Malvern Zetasizer Nano ZSP (Malvern Panalytical, Malvern, UK) with a 633 nm helium-neon laser. 50 µM AgNPs were suspended in milli-Q water, HEPES saline and HEPES glucose buffer and, after 30 minutes of incubation, each sample was measured three times at a fixed 173° back-scattering angle for the hydrodynamic diameter and 17° scatter angle for ζ potential. Note that the concentration of AgNPs used in this investigation refers to µmoles of silver per litre. The results were processed using the Malvern Zetasizer software to obtain the hydrodynamic diameter from the analysis of the autocorrelation function of the light intensity scattered by the AgNPs, and the ζ potential from the measured electrophoretic mobility using the Smoluchowski approximation. The comparison of the hydrodynamic diameter of AgNPs suspended in the different media was used to evaluate their colloidal stability.

In addition, DLS was used to evaluate the aggregation kinetics of AgNPs. For these experiments, the hydrodynamic size of the AgNPs suspended in the different buffers at various concentrations was monitored for 2 hours, taking measurements every 60 seconds.

The aggregation kinetics of colloidal suspensions can be fast, when there is not a repulsive barrier between the particles and every collision between particles leads to attachment. A slow, weakly aggregating regime occurs when the colliding particles encounter a repulsive energy barrier and only a small fraction of collisions are effective in attachment into larger aggregates. The probability of effective collisions is indicated by the attachment efficiency (α). It can be estimated by normalising the slow aggregation rate constant (k_s) to the aggregation rate constant in the fast aggregation regime (k_{fast})[31]:

$$\alpha = \frac{k_s}{k_{fast}} \quad (1)$$

The fast aggregation rate constant can be estimated using Smoluchowski's coagulation theory, where k_B is Boltzmann's constant, T is the temperature and η is the viscosity of the medium[32]:

$$k_{fast} = \frac{4k_BT}{3\eta} \quad (2)$$

The slow aggregation constant is calculated from the experimental data. The increase in hydrodynamic diameter (D_h) of AgNPs at early time was analysed using a linear least-squares regression, and the slope ($(dD_h(t))/dt)_{t\to0}$) is used for calculating k_s [31]:

$$\frac{1}{D_{h0}}\left(\frac{dD_h(t)}{dt}\right)_{t\to0} = k_sN_0\left[1+\frac{\sin(D_{h0}q)}{2D_{h0}q}\right]\left(1-\frac{1}{\delta}\right) \quad (3)$$

Here, D_{h0} is the initial hydrodynamic diameter of the single AgNPs; N_0 is the initial AgNPs concentration expressed in NPs/m^3 (see Supporting Information, table S1); δ is the relative hydrodynamic radius of a doublet (1.38) and q is the light scattering vector given by $q = 4\pi n/\lambda sin(\theta/2)$, where n is the refractive index of the medium, λ is the wavelength of light and θ is the scattering angle.

The attachment efficiency, α, permits calculation of the energy barrier, E_b, two AgNPs must overcome in a collision in order to become attached within an aggregate. The ratio of probabilities for particle attachment and particle repulsion in a collision is given by the Boltzmann factor $\alpha/(1-\alpha) = \exp(-E_b/k_BT)$.

Preparation of Large Unilamellar Vesicles (LUVs)

Carboxyfluorescein-loaded large unilamellar vesicles (LUVs) were prepared by the extrusion method. Initially, a 25 mg mL^{-1} solution of DOPC in chloroform was dried under high vacuum overnight to get a dry lipid thin film. The lipid film was then rehydrated with 500 µL of 120 mM 5(6)-carboxyfluorescein (CF) solution to form a suspension of liposomes polydisperse in size and lamellarity. Next, to break the multilamellar vesicles (MLVs) and form unilamellar liposomes, the sample was frozen in liquid nitrogen, thawed in water bath at 60°C and vortexed. This freeze-thaw-vortex cycle was carried out 10 times. The sample was subsequently extruded 11 times by passing through a 400 nm pore size polycarbonate membrane (Whatman International Ltd., Maidstone, UK) using an Avanti mini-extruder (Avanti Polar Lipids Inc.) to obtain a homogeneous population of 400 nm LUVs. Finally, the sample was passed through a Sephadex G-25 column to remove the unencapsulated CF via size exclusion chromatography. The size of the LUVs was determined by DLS and the lipid concentration by a standard phosphorus assay[33, 34].

Briefly, for the phosphorous assay 70 µL aliquots of the vesicle sample were added to sample test tubes and calibration test tubes were created using a phosphorous standard solution (0, 0.0325, 0.065, 0.114, 0.163, 0.228 µmoles phosphorous). 450 µL 8.9 N H_2SO_4 (aq) was added to each test tube and heated to 215°C for 25 minutes. The test tubes were allowed to cool before adding 150 µL H_2O_2 (30 wt%) to each one and heating at 215°C for a further 30 minutes. Test tubes were allowed to cool before adding 3.9 mL deionised water, 0.5 mL 2.5% ammonium molybdate(VI) tetrahydrate solution and 0.5 mL 10% ascorbic acid solution then heating at 100°C for 7 minutes. Once samples had cooled, the adsorption of each sample was measured at 820 nm. Phosphorous (and therefore lipid) concentrations were determined by comparison to the calibration curve created using the phosphorous standards.

Carboxyfluorescein leakage assay

The leakage assay is a technique that permits the detection of changes in membrane permeability. It is based on the self-quenching ability of the fluorophore CF when it is highly concentrated. The CF was encapsulated within LUVs at enough concentration to be self-quenched and the LUVs were exposed to different concentrations of AgNPs. A membrane damage induced by the AgNPs will produce the release of CF to the external medium where it gets diluted and consequently its fluorescence signal increase significantly. The fluorescence intensity was measured from 500 nm to 600 nm (excitation at 492 nm) using a FluoroMax-Plus spectrofluorometer (Horiba Scientific). The results were calculated from the fluorescence intensity peaks at 514 nm (I_n) and are presented as the normalized percentage of dye leakage. To calculate the fraction of dye release, a sample of LUVs before exposure to AgNPs was used as baseline signal (I_0) which was subtracted from the emission spectrum and values for complete dye leakage (I_{max}) were obtained by adding 50 µL of the surfactant Triton X-100 which causes the lysis of the LUVs and therefore the release of the 100% of CF. The normalized fraction of CF leakage (L_n) is given by:

$$L_n = \frac{I_n - I_0}{I_{max} - I_0}\ x\ 100 \qquad (4)$$

Preparation of Giant Unilamellar vesicles (GUVs)

GUVs were prepared from 0.7 mM DOPC with 0.5 mol% of 18:1 Lissamine rhodamine PE (Rh-DOPE) dissolved in chlorophorm using the electroformation method [35, 36]. Briefly, 15 µL of lipid solution were deposited as a thin layer over the conductive side of two indium-tin oxide (ITO) coated glass slides and then dried under a nitrogen stream. The ITO slides were then assembled into an electroformation chamber each in contact with a copper tape and separated by a Teflon gasket. The chamber was filled with a 300 mM sucrose solution (300 mOsm kg^{-1}) and connected to a function generator to apply an AC

electric field. The electroformation was carried out at 5 V peak to peak and 10 Hz for two hours and then the frequency was gradually reduced for approximately 10 minutes to facilitate the closure and detachment of GUVs from the surface. After electroformation, the GUVs were suspended in isotonic (unless otherwise specified) HEPES saline or HEPES glucose buffers. The osmolality of the buffer was measured using a 3320 single-sample micro-osmometer (Advanced Instruments, Norwood, UK). The GUVs observed in this study were between 5 μm and 40 μm (diameter). The GUV-based experiments were conducted at room temperature on a Zeiss LSM 880 inverted laser scanning confocal microscope. The samples were deposited on the microscope slides previously treated with a 10% BSA solution to prevent GUVs from adhering and rupturing onto the glass.

Determination of changes in morphology and membrane permeability of GUVs

Confocal laser scanning microscopy was used to monitor changes in the permeability and the morphology of GUVs induced by AgNPs. Initially, a membrane-impermeable fluorescent dye (10 kDa dextran cascade blue or CF 576 Da) was added to 200 μL of GUVs suspension, consequently the bulk solution becomes fluorescent whereas the lumen of the GUVs remains uncoloured. The microscope tile scanning option was used to scan large areas of the sample and facilitate the acquisition of statistical data. These scans were acquired before and after incubating the GUVs with different concentrations of AgNPs for 20 ± 5 minutes. The fluorescence intensity in the lumen of GUVs was quantified and normalised using the equation 4 were now L_n is the percentage of dye that leak into a particular GUV, I_0 is the average pixel intensity of the dye in the lumen of the GUVs in the unleaked control samples before adding the AgNPs, I_n is the average pixel intensity of the dye in the lumen of the particular GUV and I_{max} is the average pixel intensity of the dye in the bulk solution. Only GUVs with unilamellar appearance were analysed and just the GUVs with a normalised fluorescence intensity in their lumen higher than 20% were considered

permeable to the fluorescent molecules in the external medium. The images were analysed using the Fiji extension of ImageJ software (National Institutes of Health, Bethesda, MD) and the proportion of GUVs affected by the AgNPs was determined by manual counting.

Fluorescence recovery after photobleaching (FRAP)

Fluorescence recovery after photobleaching (FRAP) was used to investigate changes in the fluidity of the membrane. This technique consists of bleaching irreversibly a particular region of interest (ROI) with a high-intensity laser beam and then monitoring, with a low-intensity laser beam, the rate of fluorescence recovery which represents the time needed for the surrounding fluorescent molecules to diffuse into that region of interest [37]. FRAP experiments were performed on the top pole of GUVs before and after 20 ± 5 minutes of exposure to AgNPs. A circular ROI of 5 ± 0.5 µm diameter was exposed to 5 bleaching scans at 100% laser power and the recovery was monitored by recording time series of 100 frames with the confocal pinhole adjusted to 3 µm. The recovery curves were fitted with Origin Pro using the classic fluorescence recovery model [38, 39]:

$$f(t) = A\left\{exp\left(-\frac{2\tau_D}{t}\right)\left[J_0\left(\frac{2\tau_D}{t}\right) + J_1\left(\frac{2\tau_D}{t}\right)\right]\right\} \quad (5)$$

where t is time, A is the recovery level, τ_D is the half recovery time, and J_0 and J_1 are modified Bessel functions of the first kind. The diffusion coefficient (D) can then be calculated from the recovery times and the radius of the bleached region (r) using:

$$D = \frac{r^2}{4\tau_D} \quad (6)$$

Flicker spectroscopy

The membrane mechanical properties of GUVs were determined using flicker spectroscopy [40-42]. This is a non-invasive image analysis technique which quantifies the

amplitude of membrane thermal fluctuations ($\langle|u(q)|^2\rangle$) as a function of their wavenumber ($q=2\pi/l$) along the length (l) of the GUV contour. For these experiments, an osmotic relaxation of the GUVs was carried out incubating the GUVs overnight at 4º C with a hyperosmotic buffer (315 mOsm kg^{-1}). Confocal microscopy time series of 1000 frames and a resolution of 1024 x 1024 pixels were taken at the equatorial plane of single GUVs before and after 20 ± 5 minutes of exposure to AgNPs. The confocal pinhole aperture was adjusted to 0.7 µm and, to increase the scan speed, single GUVs were zoomed in upon to the maximum magnification that allows imaging of the whole vesicle. The data was analysed using MATLAB contour analysis software kindly provided by Prof. Pietro Cicuta and co-workers at the University of Cambridge, UK. This programme analyses each frame of the time series and quantifies the membrane tension (σ) and bending rigidity modulus (κ_b) by fitting the fluctuation spectrum with the following equation [42]:

$$\langle|u(q)|^2\rangle = \frac{K_B T}{2\sigma}\left(\frac{1}{q} - \frac{1}{\sqrt{\frac{\sigma}{\kappa_b} + q^2}}\right) \quad (7)$$

RESULTS

AgNPs tend to aggregate in physiological ionic strength buffer

The AgNPs employed in this investigation were coated by sodium citrate and traces of tannic acid. These AgNPs were nanospheres with a diameter of 22.4 ± 2.51 nm as determined by transmission electron microscopy (TEM) (Figure 1a). Nonetheless, the conditions of the medium can have an important influence on the biological activity of AgNPs by modifying their physicochemical properties leading, for instance, to nanoparticle dissolution, nanoparticle aggregation or interaction with organic matter [43].

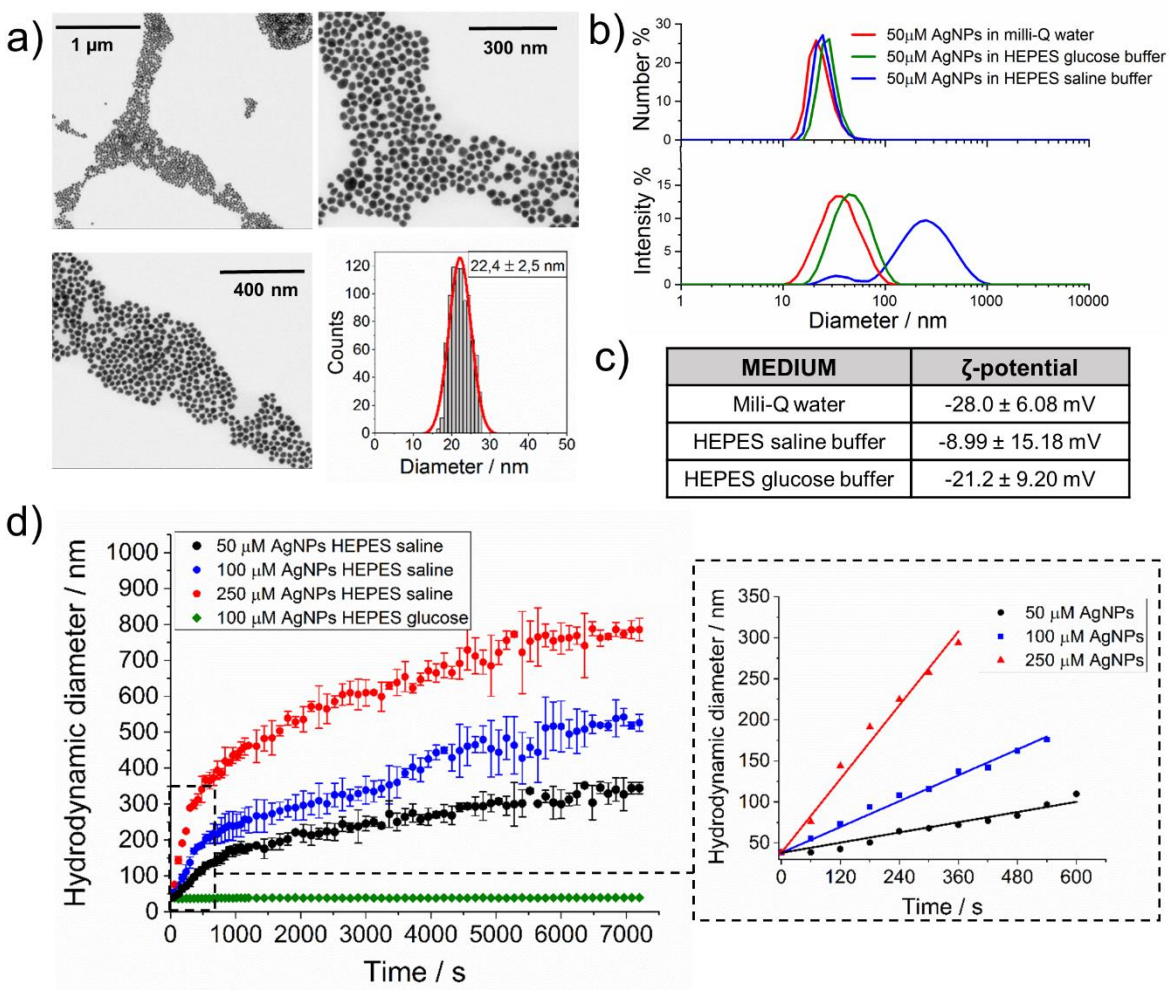

MEDIUM	ζ-potential
Mili-Q water	-28.0 ± 6.08 mV
HEPES saline buffer	-8.99 ± 15.18 mV
HEPES glucose buffer	-21.2 ± 9.20 mV

328

Figure 1. **Characterisation of AgNPs in different medium conditions .a)** TEM images show spherical AgNPs with an average diameter of 22.4 ± 2.51 nm. **b)** Dynamic light scattering (DLS) data of 50 µM AgNPs suspended in mili-Q water, HEPES saline and HEPES glucose buffer for 30 minutes. The size distribution by number (top graph) shows a monodisperse distribution of AgNPs with peaks around 25 nm, however the size distribution by intensity (bottom graph) displays similar hydrodynamic diameters of AgNPs dispersed in mili-Q water (40.25 ± 1.02 nm) and HEPES glucose buffer (43.55 ± 0.86 nm), whereas in HEPES saline buffer AgNPs show a tendency to form aggregates (199.40 ± 21.45 nm). **c)** The ζ-potential of AgNPs dispersed in mili-Q water and HEPES glucose was also similar while in HEPES saline buffer the surface charge of AgNPs becomes less negative. d) Aggregation kinetics of AgNPs. In HEPES saline buffer the hydrodynamic diameter increases with time and NP concentration. The inset plot to the right is the enlarged early time aggregation used for the calculation of the aggregation rate constant (k_s).

The colloidal stability and ζ-potential of AgNPs in physiological and low ionic strength buffers was tested using dynamic light scattering (DLS) and electrophoretic light scattering (DELSA). The aggregation of NPs can be easily detected by comparing the hydrodynamic size of AgNPs suspended in milli-Q water with their hydrodynamic size when suspended in the buffer of interest. The size distribution by intensity shows that the hydrodynamic diameter of AgNPs in HEPES glucose buffer (43.55 ± 0.86 nm) does not differs significantly from the results in milli-Q water (40.25 ± 1.02 nm), hence the NPs are stable in this buffer (Figure 1b). The larger size obtained by DLS compared to TEM is expected because while TEM measures only the physical size of the core NPs, DLS measures the hydrodynamic size which in addition to the NP core, takes into account the stabiliser coating and the electrical double layer around the NPs[44, 45]. On the contrary, these AgNPs show a tendency to form aggregates (199.40 ± 21.45 nm) when the ionic strength of the medium is high (physiological), however the size distribution by number indicates that at this concentration (50 µM) and incubation time (30 min) most of the AgNPs are still monodisperse (Figure 1b). Similarly, the ζ-potential of AgNPs is comparable in milli-Q water and HEPES glucose buffer, -28.00 ± 6.08 mV and -21.2 ± 9.20 mV respectively, whereas in HEPES saline buffer the surface charge of AgNPs becomes less negative (-8.99 ± 15.18. mV) (Figure 1c). The aggregation tendency and the less negative surface charge of AgNPs in physiological ionic strength conditions are closely related. The negative surface charge provided by the citrate coating stabilises the AgNPs suspension by electrostatic repulsions, however in HEPES saline buffer the high concentration of ions produces a screening of the surface charge that compresses the electrical double layer around the AgNPs[46-48]. Consequently, the electrostatic repulsions between AgNPs become weaker and their aggregation tendency increases.

The aggregation profile of AgNPs in HEPES saline shows a relatively fast initial increase in hydrodynamic diameter that slows down after about 10 minutes (Figure 1d). As expected, the more concentrated samples exhibit faster growth, forming larger aggregates. Analysis of the early, linear stages of aggregate growth was used to calculate the average aggregation rate constant (k_s) for AgNPs in HEPES saline buffer. Analysis of the three different concentrations of AgNPs lead to calculation of an average attachment efficiency, α = 0.016 ± 0.003. The low value of α is typical of a weakly aggregating regime where less than 2% of collisions results in aggregation. From this value of α, we calculate that the AgNPs must, on average, overcome a 4.1 k_BT energy barrier (E_b) in a collision in order to stick to each other.

The ionic strength of the medium modulates the effect of AgNPs on the membrane permeability

The effect of AgNPs on the membrane permeability was initially investigated by quantifying the release of 5(6)-carboxyfluorescein from DOPC LUVs. The carboxyfluorescein (CF) loaded DOPC LUVs (400 nm diameter) were suspended in isotonic HEPES saline buffer or HEPES glucose buffer reaching a final phospholipid concentration of 0.10 ± 0.02 μM. The LUV suspensions were then exposed to various concentrations of AgNPs (1 μM, 3 μM, 10 μM, 30 μM and 100 μM) and the fluorescence emission of each sample at 514 nm was measured every 15 minutes during a total time of 90 minutes (Figure 2a). The maximum absorption peak of these AgNPs was at 417.4 nm (Figure S1), far from the working wavelength of CF, however this peak can change due to NP aggregation. Thus, control experiments were performed comparing the fluorescence emission of samples at various concentrations of CF and the same samples plus 100 μM AgNPs to ensure that the NPs are not interfering with the fluorescence signal of CF (Figure S2). In HEPES saline buffer, the exposure of LUVs to 10 μM AgNPs produce a notable dye leakage, but at higher

AgNPs concentrations dye release from the LUVs begin to be more extensive, reaching a maximum leakage of nearly 15% and 30% after 30 minutes of incubation with 30 μM and 100 μM AgNPs, respectively. At that moment, the dye release reaches a plateau and remains stable for the next 60 minutes. In HEPES glucose buffer, after 30 minutes incubation at the highest concentrations of AgNPs (30 μM and 100 μM), the LUVs produce just a marginal dye release, which does not vary until 90 minutes of exposure when it increases slightly but does not exceed 10% CF release. Since aggregation is known to be concentration and time dependent, at lower concentrations the NPs are less aggregated. However, at the same incubation times, the highest concentrations of NPs lead to more and larger aggregates, but still in suspension, which would be able to interact with the vesicles and perturb their membrane due to their reduced solubility. At longer times, the aggregates slowly grow further until they reach a size where they are no longer colloidal, drop out of suspension and sediment to the bottom of the sample. In this way, aggregates become gradually excluded from the solution and no longer able to interact with the vesicles. These results indicate that the conditions of the surrounding environment have a pronounced influence on the interaction mechanism between AgNPs and zwitterionic phospholipid membranes.

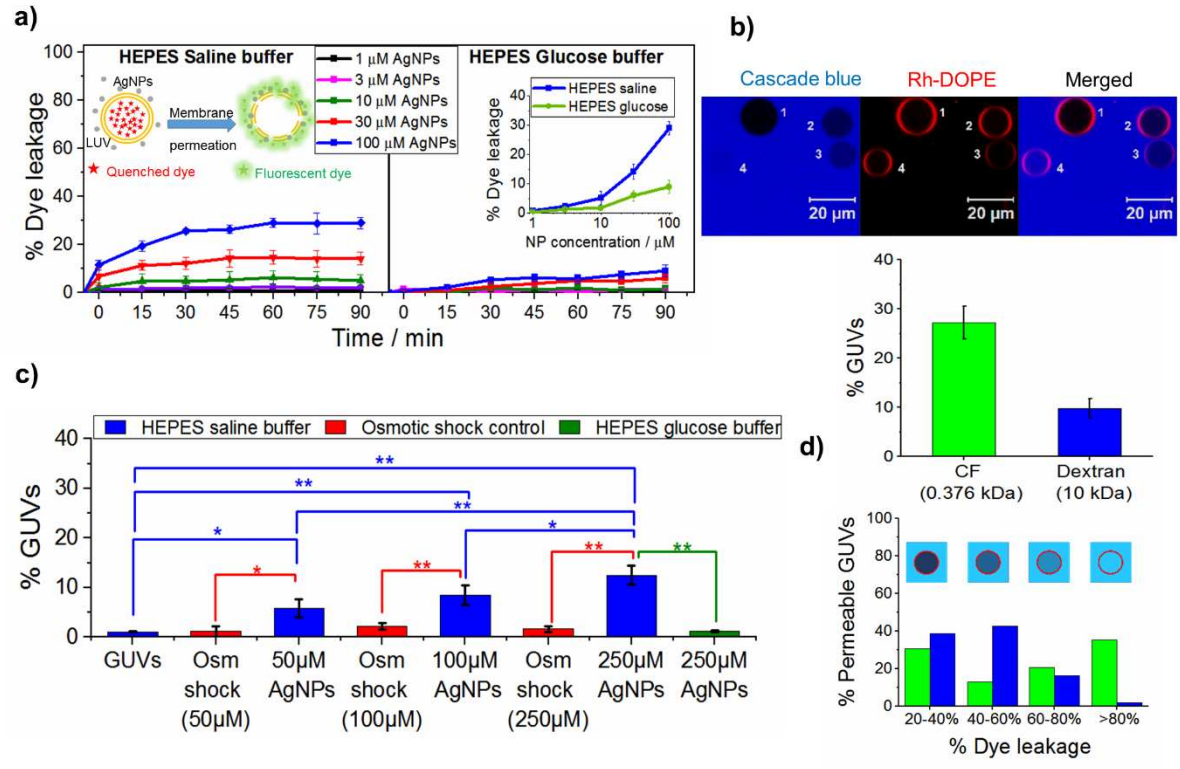

Figure 2. AgNPs in physiological ionic conditions have a more significant impact on membrane permeability. a) In HEPES saline buffer AgNPs induce a higher dose-dependent leakage of 5(6)-carboxyfluorescein (CF) from DOPC LUVs than in HEPES glucose buffer. Insets show a schematic representation of CF leakage from LUVs as well as the proportion of dye leakage as a function of NP concentration after 90 minutes of incubation. **b)** DOPC GUVs labelled with Rh-DOPE with different degrees of permeability to 10 kDa dextran labelled with cascade blue fluorophore: unleaked GUV (1), partially leaked GUVs (2 and 3) and fully leaked GUV (4). **c)** The proportion of DOPC GUVs permeable to 10 kDa dextran increases with the concentration of AgNPs in physiological ionic strength medium. Osmotic shock controls confirmed that this effect was not induced by changes in the osmolarity of the medium. In HEPES glucose buffer, the highest concentration of AgNPs does not induce a noticeable change in the number of GUVs permeable to dextran. The statistical significance was tested using a one way ANOVA with Bonferroni multiple comparisons test (*$p \leq 0.05$, **$p \leq 0.01$). **d)** Comparison between influx of CF and 10 kDa dextran into DOPC GUVs after exposure to 100 µM AgNPs. A higher proportion of GUVs become permeable to CF than to dextran. The distribution of permeable GUVs according to their level of leakage show a higher influx rate of CF than of dextran. Inset: schematic view of different levels of dye leakage. The data presented in c) and d) were obtained from the analysis of 700 ± 75 GUVs for each different condition.

The release of the dye encapsulated in the vesicles can be a consequence of different processes, from complete lysis of liposomes to the formation of nanosized pores in the membrane. To identify the mechanism behind the change in membrane permeability, we used confocal microscopy to directly observe the influx of membrane impermeable dextran molecules (10 kDa) labelled with the fluorophore Cascade blue into GUVs after incubating them for 20 ± 5 minutes with 50 μM, 100 μM and 250 μM AgNPs (Figure 2b). Additionally, control experiments were carried out adding equivalent volumes of milli-Q water to the GUVs to test the effect of a potential osmotic shock and ensure that the effects observed are indeed produced by the AgNPs. At physiological ionic strength, the exposure to AgNPs induces a dose-dependent increase in GUVs permeable to 10 kDa dextran, which is statistically significant at the three concentrations of AgNPs tested (Figure 2c). This effect is not observed in low ionic strength (HEPES glucose buffer) conditions where the exposure of the GUVs to AgNPs barely produces any change in their permeability to dextran 10 kDa. Thus, these observations demonstrate a regulating role of the medium composition on the AgNPs-membrane interactions.

The influx of large macromolecules, such as 10 kDa dextran, into the lumen of GUVs must be induced by the formation of pores in the membrane, which can vary in size and lifetime [49-51]. Confocal microscopy enables the analysis of the behaviour of individual GUVs in the sample, allowing us to quantify the specific degree of leakage in each individual vesicle observed (Figure 2b). Figure 2d compares the proportion of GUVs permeable to CF (0.37 kDa) and 10 kDa dextran after exposure to 100 μM of AgNPs as well as the distribution according to their degree of leakage. The proportion of GUVs permeable to CF molecules is nearly three times higher than to macromolecules of dextran. The distribution of permeable GUVs as a function of the normalised fluorescence intensity in their lumen show that nearly 40% of the permeable GUVs were fully filled (> 80% dye leakage) with CF after

exposure to 100 μM AgNPs whereas less than the 20% of GUVs permeable to 10 kDa dextran showed more than 60% of leakage, of which just a marginal proportion were fully leaked. According to these results, the AgNPs produce nanoscale pores in physiological ionic solutions, which allow the easier and faster transmembrane diffusion of small molecules than larger macromolecules. Moreover, the fact that just a low proportion of the GUVs get fully leaked suggest that the pores formed are transient and the membrane can self-heal, recovering its integrity and blocking further transmembrane diffusion.

AgNPs can induce the formation of intraluminal vesicles in physiological ionic strength conditions

The exposure to AgNPs produces membrane intraluminal vesicles (ILVs) in a small proportion of the GUVs when suspended in physiological ionic strength buffer. These ILVs are small vesicles filled with extravesicular bulk medium (10 kDa dextran labelled with cascade blue fluorophore) within the lumen of the GUVs. The formation of the ILVs is very fast, however some images show potential intermediate states consisting of pearling tubes (Figure 3). This phenomenon has been previously reported by Yu and Granick, who observed that aliphatic amine NPs encapsulated within DOPC GUVs adsorb onto the inner lipid leaflet of the membrane and induce an initial protrusion of large tubes followed by pearling events[52]. Montis *et al.* also observed that the exposure of POPC GUVs to cationic gold nanorods (AuNR) produce tubular lipid protrusions that breakup into pearls[25]. The experimental procedure and data analysis used for these experiments was the same employed for the estimation of dye leakage into GUVs. The proportion of GUVs with ILVs is low but statistically significant with respect to GUVs before exposure to AgNPs and the osmotic shock controls. Notably, ILVs formation does not vary significantly with the concentration of AgNPs, presenting in all cases between the 5% and 6% of GUVs observed

(Figure 3). This effect was not seen in low ionic strength buffer, hence it is also influenced by the composition of the medium.

These results suggest that the formation of ILVs is a stochastic event that has plateaued at its maximal extent by 50 μM AgNPs. We propose that this effect could be related to the aggregation of AgNPs in physiological conditions. Previous work on ZnO NPs reported that largescale aggregation leading to microscale aggregates that drop out of suspension have reduced membrane interactions[53]. The nanoscale aggregates we observe for AgNPs suggest they are more weakly aggregating and maintain their solution dispersion, this time increasing their activity at membranes. The aggregation of NPs can be considered as a stochastic process which may lead to a large number of aggregates polydisperse in size and shape. Computer simulation studies have shown that the configuration that NPs adopt to form clusters or aggregates modifies their ability to bend lipid membranes [54-57]. Therefore, the formation of ILVs could be a result from the assembly of AgNPs clusters on the GUV membrane. Nonetheless, only aggregates with a particular shape, size and orientation would be able to efficiently bend the membrane to induce pearling and ILV formation.

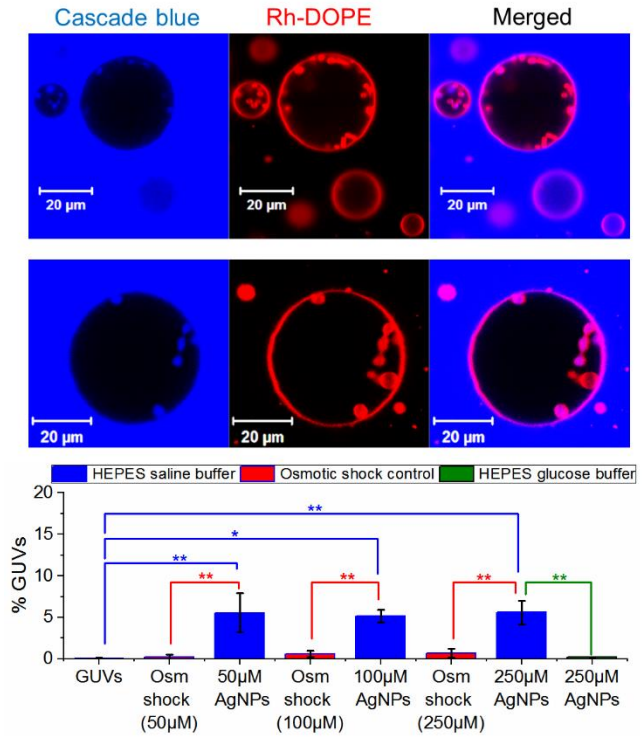

Figure 3. **AgNPs in physiological ionic conditions can induce topological changes in GUV membranes with low probability.** Small intraluminal vesicles (ILVs) and tubular structures filled with bulk solution are observed inside the GUVs upon exposure to AgNPs in physiologic ionic strength conditions. The proportion of GUVs with ILVs observed is low and similar at the three concentrations of AgNPs explored. Osmotic shock controls were performed to ensure that this effect was not induced by changes in the osmolarity of the medium. In HEPES Glucose buffer, the exposure to 250 µM of AgNPs do not favour the formation of membrane inclusions. The statistical significance was tested using a one way ANOVA with Bonferroni multiple comparisons test (*$p \leq 0.05$, **$p \leq 0.01$). The data were obtained from the analysis of 700 ± 75 GUVs for each different condition.

AgNPs slightly modifies the membrane fluidity in physiological ionic strength conditions

Fluorescence recovery after photobleaching (FRAP) was employed to investigate changes in lipid lateral mobility. The diffusion coefficients were calculated from the mobility of the fluorescent lipids (Rh-DOPE) within the membrane of GUVs estimated from the

fluorescence recovery times in a previously bleached region of the upper pole of a vesicle. The diffusion coefficient of DOPC GUVs was calculated before and after incubation with AgNPs in both high and low ionic strength buffers. Fitting of the fluorescence recovery data is well described by a single diffusion coefficient in all the conditions. Between 15 and 20 GUVs were analysed for each condition and the results are summarised in Figure 4, which show the distribution of lipid diffusion coefficients in GUVs as well as an example of FRAP recovery curve in the two media. In HEPES saline buffer, the diffusion coefficient of the DOPC lipids after exposure to 100 µM AgNPs drops by an average of 16%, from 3.02 ± 0.34 $\mu m^2 s^{-1}$ to 2.54 ± 0.31 $\mu m^2 s^{-1}$. We suggest that this subtle impact of AgNPs on the fluidity of the membrane is originated by a slight increase in the lipid packing produced by generic adsorption interactions of AgNPs on the membrane. Notably, this decrease in membrane fluidity occurs universally across all GUVs in the sample as the histograms are almost fully displaced from one another in the physiological buffer, unlike the low probability effects of poration and ILV formation seen in earlier experiments. This implies that the change in membrane fluidity in itself is not the primary mechanism that gives rise to these other membrane perturbations.

In low ionic strength conditions, the AgNPs barely modify the lipid lateral mobility suggesting negligible or very transient adsorption of AgNPs onto the membrane under these conditions. Interestingly, the average diffusion coefficient of DOPC GUVs in these conditions (2.54 ± 0.31 $\mu m^2 s^{-1}$) is lower than in high ionic strength buffer. These data suggest that the ionic strength of the medium could not be the only environmental condition modulating the interaction mechanism between the AgNPs and the membrane, but also the presence of high concentrations of sugars might be protecting the membrane. Previous studies have reported that sugars decrease the lipid lateral diffusion in a concentration-dependent manner using Fluorescence Correlation Spectroscopy (FCS) [58]. Therefore, we attributed the

lower membrane fluidity in low ionic strength buffer to the high concentration of glucose in the medium.

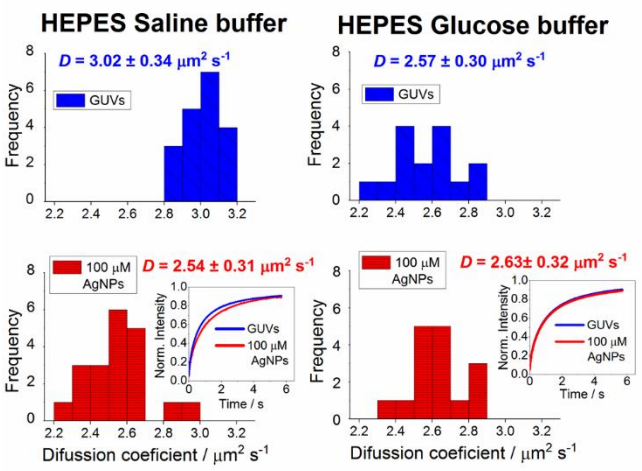

Figure 4. AgNPs in physiological salt conditions decrease membrane fluidity but have no impact in low ionic strength conditions. Distribution of diffusion coefficients obtained from FRAP recovery curves of DOPC GUVs in HEPES saline buffer (high ionic strength) and HEPES glucose buffer (low ionic strength) before and after exposure to 100 μM AgNPs. *D* values indicate the mean diffusion coefficient calculated in each condition. In HEPES saline buffer, AgNPs induce a slight but statistically significant decrease in lipid lateral diffusion. In low ionic strength medium the membrane fluidity of DOPC GUVs is lower than in HEPES saline and does not change after incubation with AgNPs. Insets show examples of FRAP recovery curves obtained in each condition. The number of GUVs analysed in each data set were: GUVs (HEPES saline), n=19; GUVs + 100 μM AgNPs (HEPES saline), n=18; GUVs (HEPES glucose), n=15; GUVs + 100μM AgNPs (HEPES glucose), n=16.

AgNPs considerably affect the mechanical properties of a sub-population of GUVs in physiological ionic strength buffer

The ability of AgNPs to produce membrane invaginations suggest that these NPs might modify the mechanical properties of the membrane. Flicker spectroscopy experiments were performed to quantify the distribution of membrane tension (σ) and bending modulus

(κ_b) of GUV membranes. This technique has a limitation in spatiotemporal resolution which does not allow us to calculate accurately the amplitude of membrane fluctuations ($\langle|u(q)|^2\rangle$) of high-tension GUVs within a broad enough range of wavenumbers (q) [59]. This issue was circumvented by the osmotic relaxation of GUVs which decreases the tension of the membrane, increasing the amplitude of the membrane's thermal undulations and therefore making the fitting of the power spectrum more reliable. Additionally, the osmotic pressure of the AgNPs suspension was balanced with sucrose until isotonic to the experimental medium to prevent changes in the osmolarity of the medium during the experiment.

As expected, in low ionic strength glucose buffer AgNPs do not induce any significant change in either the tension or the bending rigidity of the membrane. In high ionic strength (physiological) conditions, the addition of 100 μM AgNPs to the osmotically relaxed GUVs induces subtle changes in the mechanical properties of the membrane. The distribution of both the tension and the bending rigidity values become wider after the incubation of GUVs with AgNPs. We observe a rise in the mean membrane tension, which despite not seeming to be a drastic change, is statistically significant ($p < 0.01$) (Figure 5a). This increase in membrane tension is accompanied by a small decrease in membrane rigidity, nevertheless this latter change does not show statistical significance (Figure 5b). Interestingly, these changes in membrane mechanics are not produced by a global effect on every GUV in the sample, but arise from profound changes in membrane tension and bending rigidity of just a fraction of the GUVs analysed (Figure 5c). These results could be directly related to the formation of membrane pores, invaginations and ILVs, described early, which also only occur in a small sub-population of the GUVs. A recent study has shown that formation of ILVs by the endosomal sorting complex required for transport (ESCRT) produces a significant increase in the membrane tension of GUVs originated by the removal of excess membrane surface area [60]. Furthermore, the increase of the membrane tension is known to

favour the membrane poration[61-63], and therefore could favour the membrane permeation effect induced by AgNPs.

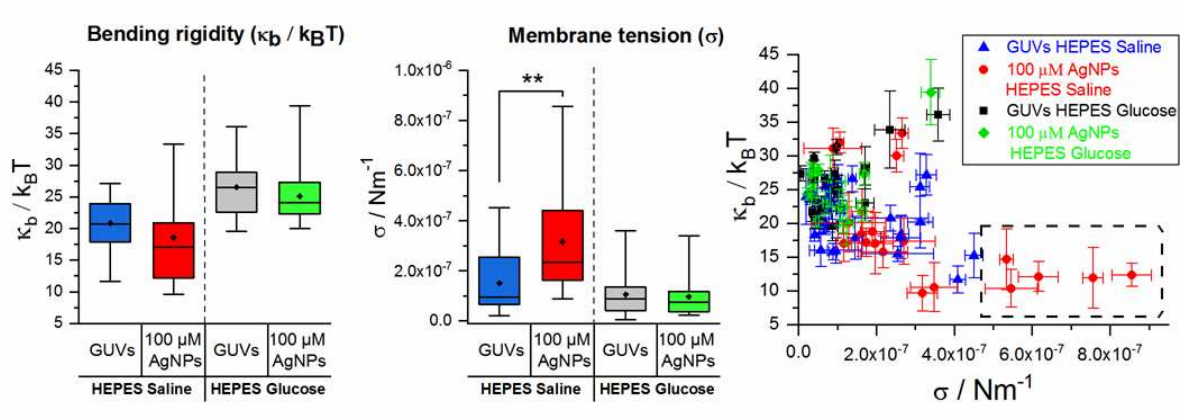

Figure 5. AgNPs in physiological ionic conditions significantly impact the membrane mechanical properties of a sub-population of GUVs. a) In HEPES saline, 100 µM AgNPs induce a broader distribution and a slight shift in bending rigidity (κ_b / k_BT) which is not statistically significant. In low ionic strength buffer the bending rigidity barely changes. **b)** In HEPES glucose buffer the membrane tension (σ) does not vary after exposure of GUVs to 100 µM AgNPs whereas is HEPES saline a significant change in membrane tension is observed (**$p \leq 0.01$, ANOVA with Bonferroni multiple comparisons test). **c)** The plot of bending rigidity against membrane tension show that the majority of GUVs in all conditions have similar membrane tension (>5x10^{-7} Nm^{-1}) and bending rigidity (15 – 35 κ_b/k_BT). However, a small proportion of GUVs in HEPES saline experience a great change in membrane tension after exposure to 100 µM AgNPs which is also associated to a small decrease in bending rigidity (dashed box). These GUVs show a membrane tension higher than 5x10^{-7} Nm^{-1} and a bending rigidity between 10 and 15 κ_b/k_BT. The number of GUVs analysed in each data set were: GUVs (HEPES saline), n=31; GUVs + 100 µM AgNPs (HEPES saline), n=27; GUVs (HEPES glucose), n=25; GUVs + 100µM AgNPs (HEPES glucose), n=25.

Finally, control experiments adding equivalent concentrations of $AgNO_3$ to the vesicles were carried out to study a possible maximal effect of dissolution of Ag^+ ions on the membrane integrity (Figure S3 a-d). These results demonstrate that changes in membrane

permeability, fluidity and mechanical properties are not caused by any release of Ag^+ ions from the AgNPs, hence we confidently conclude that all the membrane perturbations observed in this investigation are produced directly by the weakly aggregating AgNPs.

DISCUSSION

The behaviour of nanomaterials in biological systems is governed by their physicochemical properties, nonetheless these properties are susceptible to change once the NPs enter biological media. The results presented in this work firstly evidence a significant impact of the medium conditions on the surface charge and colloidal stability of AgNPs. The citrate coating of AgNPs gives them a negative surface charge and stabilises the colloidal suspension in low ionic strength media through electrostatic double-layer repulsions. However, the high concentration of ions in physiological conditions modifies the ζ-potential of AgNPs and promotes their aggregation making the NPs less negatively charged. In this medium, Na^+ ions screen the negative surface charge and decreases the inter-particle repulsive force to a thermally accessible energy barrier of 4.1 k_BT, thereby facilitating the concentration dependent aggregation of AgNPs [64, 65]. The analysis of the aggregation kinetics of AgNPs indicates a weak aggregation regime with 1.6% of AgNP collisions resulting in an aggregation event and where most of the aggregates are still in suspension at the experimental incubation times.

Several previous investigations have focused on the effect of the attachment of proteins to the NP surface (protein corona) on the biological activities of NPs [53, 66-71], however comparatively less attention has been paid to other properties of the medium, such as pH or ionic strength, which can also alter the physicochemical properties of NPs and their biointeractions. Our data show that in high (physiological) ionic strength conditions, AgNPs induce subtle but important effects on the physicochemical properties of the membrane, whereas in low ionic strength buffer the membrane maintains its integrity after exposure to

555 AgNPs. Therefore, the buffer conditions modify the interactions of AgNPs acting at the
556 nanobio interface and hence modulate their interaction with membranes. Control
557 experiments also show that any membrane perturbation observed is not caused by the
558 dissolution of Ag^+ ions from the AgNPs.

559 At pH 7.4, the DOPC membrane carries a slight negative charge [72]. Thus, in a low
560 ionic strength environments, electrostatic repulsion between AgNPs and the DOPC bilayer
561 may dominate over other attractive forces, preventing significant interaction. However, when
562 the ionic strength increases, the screening of surface charge of AgNPs decrease
563 electrostatic repulsive forces between the NPs and the membrane, increasing the likelihood
564 of more significant interaction. In addition, the loss of colloidal stability and weak aggregation
565 behaviour of AgNPs makes them less soluble and more surface active, further increasing
566 membrane interactions. This modulatory effect of the ionic strength of the medium on the
567 AgNPs-membrane interaction has been reported earlier by Wang *et al*, who, using quartz
568 crystal microbalance with dissipation (QCM-D), found that the deposition rates of AgNPs on
569 DOPC supported lipid bilayers (SLBs) increases when the concentration of salt in the
570 medium rises [73]. A similar electrostatically-mediated interaction was reported by Li and
571 Malmstadt for cationic polystyrene NPs (PNPs) which interact weakly with the membrane as
572 the ionic strength of the medium increases [49].

573 In physiological conditions, we observe that AgNPs induce changes in membrane
574 permeability and can form membrane invaginations such as ILVs. Several studies have
575 shown the ability of eukaryotic, bacterial and virus proteins as well as antibacterial peptides
576 and NPs to change the morphology of the membrane and form invaginations and ILVs
577 without the need of cellular endocytic mechanisms or external sources of energy [25, 52, 60, 74-
578 77]. Generally the interaction of single proteins or particles is not strong enough to induce
579 these large deformations of the membrane and thus many molecules or particles must

cooperate to bend the membrane [54, 75]. For instance, the clustering of Gb3-binding B subunit of the bacterial Shiga toxin (STxB) can induce membrane invagination in artificial model membranes, however these invaginations are not observed when the clustering is inhibited [74]. We propose that single AgNPs do not possess enough energy to bend the membrane, nonetheless the formation of NP clusters of a particular size and shape will increase their ability to deform the membrane and produce invaginations and ILVs. The formation of these structures removes excess membrane, which, along with the pressure generated by the AgNPs that adhere onto the membrane, increases the membrane tension and can lead to membrane poration [49]. The increase in membrane tension is also known to be the driving force of opening of pores which will in turn produce membrane permeation, causing the membrane translocation of impermeable dextran probes and the relaxation of the membrane tension. The lifetime of membrane pores is usually short because as the membrane tension relaxes, the line tension at the pore edge drives closure of the pore [61, 78]. The size of the pore defines the minimum size of the molecules that can diffuse across the membrane. The higher permeability to carboxyfluorescein (0.37 kDa) than to dextran (10 kDa) observed in our experiments represents the presence of nanoscale pores in the membrane as a result of the AgNPs. Furthermore, the fact that most of the GUVs observed were not fully leaked indicates these pores are transient.

In general, toxicology studies focus on terminal effects where the analytes induce severe damages in the membrane or other cellular components that lead to cell death. However, other subtle effects in the physicochemical properties of the membrane can also have biological importance. Cells are able to sense mechanical stimuli and convert them into intracellular biochemical signals to adapt to their microenvironment [79]. Mechanical forces can modify the mechanical and dynamical properties of the membrane, which in turn can induce conformational changes in membrane proteins, such as ion channels[80], G-

protein coupled receptors (GPCRs) [81-83] and integrins[84]. These proteins trigger metabolic cascades that lead to different cellular responses such as cell migration, differentiation, and proliferation[85, 86]. In endothelial cells for instance, the plasma membrane senses haemodynamical forces generated by the blood activating downstream signalling pathways related with inflammatory responses, regulation of blood pressure or coagulation processes [87]. Another important example of mechanical sensing and transduction is the Hippo pathway, which controls organ growth by regulating cell proliferation [88]. The mechanical stress applied to the plasma membrane modulates the actin cytoskeleton and activate GPCRs. This begins a complex signal pathway that eventually activates the proto-oncogenes proteins YAP/TAZ which translocate from the cytoplasm to the nucleus and induce cell proliferation [89]. Prolonged mechanical stress can lead to an overexpression of YAP/TAZ promoting unregulated cell proliferation and eventually oncogenesis [88, 89]. Therefore, even small changes in the mechanical and dynamical properties of the membrane, such as the ones produced by AgNPs, can induce multiple cellular responses which lead to a myriad of processes encompassing from inflammatory responses to the development of serious diseases.

Biological fluids are complex and crowded with biomolecules which can interact with the NPs in a non-specific manner and modulate their behaviour. Thereby, the biological interactions of NPs can be influenced by multiple external factors. These factors can be simulated and controlled *in vitro*, for instance introducing proteins to investigate the formation of protein coronas and their effect in NP-membrane interactions. Another factor that would be interesting to study is the impact of excluded volume effects generated by macromolecular crowding on these interactions. This phenomenon is known to promote protein-protein interactions [90], and the binding of proteins to the membrane [91], thus it is likely to influence the interaction between NPs and the membrane.

CONCLUSIONS

To summarise, here we show the significant impact that the ionic strength of the medium have on the physicochemical properties of AgNPs and their interactions with biomembranes. From our results we propose that monodisperse AgNPs are non-interacting and could be safely exploited as imaging contrast agents for diagnosis and cancer theranostics. However, the aggregation of AgNPs would lead to two different possibilities: i) large aggregates precipitate and are expelled from the solution and do not interact with the membrane. These large aggregates are expected to be highly toxic because they are more difficult to be transported in the blood and can be accumulated in certain organs before reaching their specific targets and produce severe damage [20]. ii) Smaller aggregates become more membrane active than monodisperse AgNPs increasing the tension of the membrane and opening pores. The formation of transient pores offers opportunities in transfection technologies but at the same time raises nanotoxicology concerns.

SUPPORTING INFORMATION

UV-Vis spectrum of AgNPs suspended in mili-Q water; conversion of AgNPs concentration from μmolar Ag to number of particles/m^3; leakage assay interference control; control experiments on the effect of Ag^+ in membrane permeability, membrane remodelling, membrane fluidity and membrane mechanics.

ACKNOWLEDGEMENTS

This work was funded by the E.U. Horizon 2020 project HISENTS (GA No. 685817). MAP acknowledges funding from an endowed PhD scholarship at the University of Leeds.

REFERENCES

(1) Srivastava, V., Gusain, D., and Sharma, Y. C. (2015) Critical Review on the Toxicity of Some Widely Used Engineered Nanoparticles. *Industrial & Engineering Chemistry Research 54*, 6209-6233.

(2) Zhang, L., Gu, F. X., Chan, J. M., Wang, A. Z., Langer, R. S., and Farokhzad, O. C. (2008) Nanoparticles in medicine: Therapeutic applications and developments. *Clinical Pharmacology & Therapeutics 83*, 761-769.

(3) Rascol, E., Devoisselle, J. M., and Chopineau, J. (2016) The relevance of membrane models to understand nanoparticles-cell membrane interactions. *Nanoscale 8*, 4780-4798.

(4) Singla, R., Sharma, C., Shukla, A. K., and Acharya, A. (2019) Toxicity Concerns of Therapeutic Nanomaterials. *Journal of Nanoscience and Nanotechnology 19*, 1889-1907.

(5) Barbalinardo, M., Caicci, F., Cavallini, M., and Gentili, D. (2018) Protein Corona Mediated Uptake and Cytotoxicity of Silver Nanoparticles in Mouse Embryonic Fibroblast. *Small 14*, 1801219.

(6) Dillip, G. R., Banerjee, A. N., Sreekanth, T. V. M., Anitha, V. C., and Joo, S. W. (2017) In vitro cytotoxicity of in-situ synthesized zinc oxide anchored graphitic carbon nanofiber on HeLa cells. *Materials Science in Semiconductor Processing 59*, 87-92.

(7) Kim, I. Y., Joachim, E., Choi, H., and Kim, K. (2015) Toxicity of silica nanoparticles depends on size, dose, and cell type. *Nanomedicine-Nanotechnology Biology and Medicine 11*, 1407-1416.

(8) Calderon-Jimenez, B., Johnson, M. E., Bustos, A. R. M., Murphy, K. E., Winchester, M. R., and Baudrit, J. R. V. (2017) Silver Nanoparticles: Technological Advances, Societal Impacts, and Metrological Challenges. *Frontiers in Chemistry 5*, 6.

(9) Vance, M. E., Kuiken, T., Vejerano, E. P., McGinnis, S. P., Hochella, M. F., Rejeski, D., and Hull, M. S. (2015) Nanotechnology in the real world: Redeveloping the nanomaterial consumer products inventory. *Beilstein Journal of Nanotechnology 6*, 1769-1780.

(10) Sotiriou, G. A., and Pratsinis, S. E. (2011) Engineering nanosilver as an antibacterial, biosensor and bioimaging material. *Current Opinion in Chemical Engineering 1*, 3-10.

(11) Piella, J., Bastus, N. G., and Puntes, V. (2017) Modeling the Optical Responses of Noble Metal Nanoparticles Subjected to Physicochemical Transformations in Physiological Environments: Aggregation, Dissolution and Oxidation. *Zeitschrift Fur Physikalische Chemie-International Journal of Research in Physical Chemistry & Chemical Physics 231*, 33-50.

(12) Li, Y. N., Chang, Y. T., Lian, X. F., Zhou, L. Q., Yu, Z. Q., Wang, H. X., and An, F. F. (2018) Silver Nanoparticles for Enhanced Cancer Theranostics: In Vitro and In Vivo Perspectives. *Journal of Biomedical Nanotechnology 14*, 1515-1542.

(13) Dubey, P., Matai, I., Kumar, S. U., Sachdev, A., Bhushan, B., and Gopinath, P. (2015) Perturbation of cellular mechanistic system by silver nanoparticle toxicity: Cytotoxic, genotoxic and epigenetic potentials. *Advances in Colloid and Interface Science 221*, 4-21.

(14) Carlson, C., Hussain, S. M., Schrand, A. M., Braydich-Stolle, L. K., Hess, K. L., Jones, R. L., and Schlager, J. J. (2008) Unique Cellular Interaction of Silver Nanoparticles: Size-Dependent Generation of Reactive Oxygen Species. *Journal of Physical Chemistry B 112*, 13608-13619.

(15) Mukherjee, S. G., O'Claonadh, N., Casey, A., and Chambers, G. (2012) Comparative in vitro cytotoxicity study of silver nanoparticle on two mammalian cell lines. *Toxicology in Vitro 26*, 238-251.

(16) Xue, Y. Y., Zhang, T., Zhang, B. Y., Gong, F., Huang, Y. M., and Tang, M. (2016) Cytotoxicity and apoptosis induced by silver nanoparticles in human liver HepG2 cells in different dispersion media. *Journal of Applied Toxicology 36*, 352-360.

(17) Zou, Z. Z., Chang, H. C., Li, H. L., and Wang, S. M. (2017) Induction of reactive oxygen species: an emerging approach for cancer therapy. *Apoptosis 22*, 1321-1335.

(18) Volker, C., Kampken, I., Boedicker, C., Oehlmann, J., and Oetken, M. (2015) Toxicity of silver nanoparticles and ionic silver: Comparison of adverse effects and potential toxicity mechanisms in the freshwater clam Sphaerium corneum. *Nanotoxicology 9*, 677-685.

(19) Ahmed, K. B. R., Nagy, A. M., Brown, R. P., Zhang, Q., Malghan, S. G., and Goering, P. L. (2017) Silver nanoparticles: Significance of physicochemical properties and assay interference on the interpretation of in vitro cytotoxicity studies. *Toxicology in Vitro 38*, 179-192.

(20) Casals, E., Gonzalez, E., and Puntes, V. F. (2012) Reactivity of inorganic nanoparticles in biological environments: insights into nanotoxicity mechanisms. *Journal of Physics D-Applied Physics 45*, 443001.

(21) Nel, A. E., Madler, L., Velegol, D., Xia, T., Hoek, E. M. V., Somasundaran, P., Klaessig, F., Castranova, V., and Thompson, M. (2009) Understanding biophysicochemical interactions at the nano-bio interface. *Nature Materials 8*, 543-557.

(22) Zhang, S. W., Nelson, A., and Beales, P. A. (2012) Freezing or Wrapping: The Role of Particle Size in the Mechanism of Nanoparticle-Biomembrane Interaction. *Langmuir 28*, 12831-12837.

(23) Chithrani, B. D., Ghazani, A. A., and Chan, W. C. W. (2006) Determining the size and shape dependence of gold nanoparticle uptake into mammalian cells. *Nano Letters 6*, 662-668.

(24) Moghadam, B. Y., Hou, W. C., Corredor, C., Westerhoff, P., and Posner, J. D. (2012) Role of Nanoparticle Surface Functionality in the Disruption of Model Cell Membranes. *Langmuir 28*, 16318-16326.

(25) Montis, C., Generini, V., Boccalini, G., Bergese, P., Bani, D., and Berti, D. (2018) Model lipid bilayers mimic non-specific interactions of gold nanoparticles with macrophage plasma membranes. *Journal of Colloid and Interface Science 516*, 284-294.

(26) Werner, M., Auth, T., Beales, P. A., Fleury, J. B., Hook, F., Kress, H., Van Lehn, R. C., Muller, M., Petrov, E. P., Sarkisov, L., Sommer, J. U., and Baulin, V. A. (2018) Nanomaterial interactions with biomembranes: Bridging the gap between soft matter models and biological context. *Biointerphases 13*, 028501.

(27) Behzadi, S., Serpooshan, V., Tao, W., Hamaly, M. A., Alkawareek, M. Y., Dreaden, E. C., Brown, D., Alkilany, A. M., Farokhzad, O. C., and Mahmoudi, M. (2017) Cellular uptake of nanoparticles: journey inside the cell. *Chemical Society Reviews 46*, 4218-4244.

(28) Beales, P. A., Ciani, B., and Cleasby, A. J. (2015) Nature's lessons in design: nanomachines to scaffold, remodel and shape membrane compartments. *Physical Chemistry Chemical Physics 17*, 15489-15507.

(29) Le, M. T., Litzenberger, J. K., and Prenner, E. J. (2011) Biomimetic model membrane systems serve as increasingly valuable in vitro tools, In *Advances in Biomimetics*, pp 251-276, InTech.

(30) Bastus, N. G., Merkoci, F., Piella, J., and Puntes, V. (2014) Synthesis of Highly Monodisperse Citrate-Stabilized Silver Nanoparticles of up to 200 nm: Kinetic Control and Catalytic Properties. *Chemistry of Materials 26*, 2836-2846.

(31) Chen, K. L., Mylon, S. E., and Elimelech, M. (2006) Aggregation kinetics of alginate-coated hematite nanoparticles in monovalent and divalent electrolytes. *Environmental Science & Technology 40*, 1516-1523.

(32) Norde, W. (2003) *Colloids and Interfaces in Life Sciences*, Marcel Dekker, Inc, New York.

(33) Chen, P. S., Toribara, T. Y., and Warner, H. (1956) Microdetermination of phosphorus. *Analytical Chemistry 28*, 1756-1758.

(34) Fiske, C. H., and Subbarow, Y. (1925) The colorimetric determination of phosphorus. *Journal of Biological Chemistry 66*, 375-400.

(35) Angelova, M. I., Soleau, S., Meleard, P., Faucon, J. F., and Bothorel, P. (1992) Preparation of giant vesicles by external ac electric-fields. Kinetics and applications. *Trends in Colloid and Interface Science VI 89*, 127-131.

(36) Meleard, P., Bagatolli, L. A., and Pott, T. (2009) Giant unilamellar vesicle electroformation: from lipid mixtures to native membranes under physiological conditions. *Methods in Enzymology Liposomes, Pt G 465*, 161-176.

(37) Pincet, F., Adrien, V., Yang, R., Delacotte, J., Rothman, J. E., Urbach, W., and Tareste, D. (2016) FRAP to Characterize Molecular Diffusion and Interaction in Various Membrane Environments. *Plos One 11*, e0158457.

(38) Soumpasis, D. M. (1983) Theoretical analysis of fluorescence photobleaching recovery experiments. *Biophysical Journal 41*, 95-97.

(39) Axelrod, D., Koppel, D. E., Schlessinger, J., Elson, E., and Webb, W. W. (1976) Mobility measurement by analysis of fluorescence photobleaching recovery kinetics. *Biophysical Journal 16*, 1055-1069.

(40) Rautu, S. A., Orsi, D., Di Michele, L., Rowlands, G., Cicuta, P., and Turner, M. S. (2017) The role of optical projection in the analysis of membrane fluctuations. *Soft Matter 13*, 3480-3483.

(41) Bassereau, P., Sorre, B., and Levy, A. (2014) Bending lipid membranes: Experiments after W. Helfrich's model. *Advances in Colloid and Interface Science 208*, 47-57.

(42) Pecreaux, J., Dobereiner, H. G., Prost, J., Joanny, J. F., and Bassereau, P. (2004) Refined contour analysis of giant unilamellar vesicles. *European Physical Journal E 13*, 277-290.

(43) Bastus, N. G., Casals, E., Vazquez-Campos, S., and Puntes, V. (2008) Reactivity of engineered inorganic nanoparticles and carbon nanostructures in biological media. *Nanotoxicology 2*, 99-112.

(44) Diegoli, S., Manciulea, A. L., Begum, S., Jones, I. P., Lead, J. R., and Preece, J. A. (2008) Interaction between manufactured gold nanoparticles and naturally occurring organic macromolecules. *Science of the Total Environment 402*, 51-61.

(45) Cumberland, S. A., and Lead, J. R. (2009) Particle size distributions of silver nanoparticles at environmentally relevant conditions. *Journal of Chromatography A 1216*, 9099-9105.

(46) Huynh, K. A., and Chen, K. L. (2011) Aggregation Kinetics of Citrate and Polyvinylpyrrolidone Coated Silver Nanoparticles in Monovalent and Divalent Electrolyte Solutions. *Environmental Science & Technology 45*, 5564-5571.

(47) Prathna, T. C., Chandrasekaran, N., and Mukherjee, A. (2011) Studies on aggregation behaviour of silver nanoparticles in aqueous matrices: Effect of surface functionalization and matrix composition. *Colloids and Surfaces a-Physicochemical and Engineering Aspects 390*, 216-224.

(48) Jang, M. H., Lee, S., and Hwang, Y. S. (2015) Characterization of Silver Nanoparticles under Environmentally Relevant Conditions Using Asymmetrical Flow Field-Flow Fractionation (AF4). *Plos One 10*, e0143149.

(49) Li, S., and Malmstadt, N. (2013) Deformation and poration of lipid bilayer membranes by cationic nanoparticles. *Soft Matter 9*, 4969-4976.

(50) Leite, N. B., Aufderhorst-Roberts, A., Palma, M. S., Connell, S. D., Neto, J. R., and Beales, P. A. (2015) PE and PS Lipids Synergistically Enhance Membrane Poration by a Peptide with Anticancer Properties. *Biophysical Journal 109*, 936-947.

(51) Bergstrom, C. L., Beales, P. A., Lv, Y., Vanderlick, T. K., and Groves, J. T. (2013) Cytochrome c causes pore formation in cardiolipin-containing membranes. *Proceedings of the National Academy of Sciences of the United States of America 110*, 6269-6274.

(52) Yu, Y., and Granick, S. (2009) Pearling of Lipid Vesicles Induced by Nanoparticles. *Journal of the American Chemical Society 131*, 14158-14159.

(53) Churchman, A. H., Wallace, R., Milne, S. J., Brown, A. P., Brydson, R., and Beales, P. A. (2013) Serum albumin enhances the membrane activity of ZnO nanoparticles. *Chemical Communications 49*, 4172-4174.

(54) Reynwar, B. J., Illya, G., Harmandaris, V. A., Muller, M. M., Kremer, K., and Deserno, M. (2007) Aggregation and vesiculation of membrane proteins by curvature-mediated interactions. *Nature 447*, 461-464.

(55) Spangler, E. J., Kumar, P. B. S., and Laradji, M. (2018) Stability of membrane-induced self-assemblies of spherical nanoparticles. *Soft Matter 14*, 5019-5030.

(56) Saric, A., and Cacciuto, A. (2012) Fluid Membranes Can Drive Linear Aggregation of Adsorbed Spherical Nanoparticles. *Physical Review Letters 108*, 118101.

(57) Saric, A., and Cacciuto, A. (2012) Mechanism of Membrane Tube Formation Induced by Adhesive Nanocomponents. *Physical Review Letters 109*, 188101.

(58) van den Bogaart, G., Hermans, N., Krasnikov, V., de Vries, A. H., and Poolman, B. (2007) On the decrease in lateral mobility of phospholipids by sugars. *Biophysical Journal 92*, 1598-1605.

(59) Amjad, O. A., Mognetti, B. M., Cicuta, P., and Di Michele, L. (2017) Membrane Adhesion through Bridging by Multimeric Ligands. *Langmuir 33*, 1139-1146.

(60) Booth, A., Marklew, C. J., Ciani, B., and Beales, P. A. (2019) In Vitro Membrane Remodeling by ESCRT is Regulated by Negative Feedback from Membrane Tension. *iScience 15*, 173-184.

(61) Karatekin, E., Sandre, O., Guitouni, H., Borghi, N., Puech, P. H., and Brochard-Wyart, F. (2003) Cascades of transient pores in giant vesicles: Line tension and transport. *Biophysical Journal 84*, 1734-1749.

(62) Akimov, S. A., Volynsky, P. E., Galimzyanov, T. R., Kuzmin, P. I., Pavlov, K. V., and Batishchev, O. V. (2017) Pore formation in lipid membrane II: Energy landscape under external stress. *Scientific Reports 7*, 12509.

(63) Fuertes, G., Garcia-Saez, A. J., Esteban-Martin, S., Gimenez, D., Sanchez-Munoz, O. L., Schwille, P., and Salgado, J. (2010) Pores Formed by Bax alpha 5 Relax to a Smaller Size and Keep at Equilibrium. *Biophysical Journal 99*, 2917-2925.

(64) Delay, M., Dolt, T., Woellhaf, A., Sembritzki, R., and Frimmel, F. H. (2011) Interactions and stability of silver nanoparticles in the aqueous phase: Influence of natural organic matter (NOM) and ionic strength. *Journal of Chromatography A 1218*, 4206-4212.

(65) Velegol, D. (2007) Assembling colloidal devices by controlling interparticle forces. *Journal of Nanophotonics 1*, 012502.

(66) Montis, C., Maiolo, D., Alessandri, I., Bergese, P., and Berti, D. (2014) Interaction of nanoparticles with lipid membranes: a multiscale perspective. *Nanoscale 6*, 6452-6457.

(67) Lee, Y. K., Choi, E. J., Webster, T. J., Kim, S. H., and Khang, D. (2015) Effect of the protein corona on nanoparticles for modulating cytotoxicity and immunotoxicity. *International Journal of Nanomedicine 10*, 97-112.

(68) Wei, X., Qu, X., Ding, L., Hu, J., and Jiang, W. (2016) Role of bovine serum albumin and humic acid in the interaction between SiO2 nanoparticles and model cell membranes. *Environmental Pollution 219*, 1-8.

(69) Di Silvio, D., Maccarini, M., Parker, R., Mackie, A., Fragneto, G., and Bombelli, F. B. (2017) The effect of the protein corona on the interaction between nanoparticles and lipid bilayers. *Journal of Colloid and Interface Science 504*, 741-750.

(70) Anderson, C. R., Gnopo, Y. D. M., Gambinossi, F., Mylon, S. E., and Ferri, J. K. (2018) Modulation of cell responses to Ag-(MeO(2)MA-co-OEGMA): Effects of nanoparticle surface hydrophobicity and serum proteins on cellular uptake and toxicity. *Journal of Biomedical Materials Research Part A 106*, 1061-1071.

(71) Lesniak, A., Salvati, A., Santos-Martinez, M. J., Radomski, M. W., Dawson, K. A., and Aberg, C. (2013) Nanoparticle Adhesion to the Cell Membrane and Its Effect on Nanoparticle Uptake Efficiency. *Journal of the American Chemical Society 135*, 1438-1444.

(72) Yi, P., and Chen, K. L. (2013) Interaction of Multiwalled Carbon Nanotubes with Supported Lipid Bilayers and Vesicles as Model Biological Membranes. *Environmental Science & Technology 47*, 5711-5719.

(73) Wang, Q. Y., Lim, M. H., Liu, X. T., Wang, Z. W., and Chen, K. L. (2016) Influence of Solution Chemistry and Soft Protein Coronas on the Interactions of Silver Nanoparticles with Model Biological Membranes. *Environmental Science & Technology 50*, 2301-2309.

(74) Romer, W., Berland, L., Chambon, V., Gaus, K., Windschiegl, B., Tenza, D., Aly, M. R. E., Fraisier, V., Florent, J. C., Perrais, D., Lamaze, C., Raposo, G., Steinem, C., Sens, P., Bassereau, P., and Johannes, L. (2007) Shiga toxin induces tubular membrane invaginations for its uptake into cells. *Nature 450*, 670-U673.

(75) Praper, T., Sonnen, A. F. P., Kladnik, A., Andrighetti, A. O., Viero, G., Morris, K. J., Volpi, E., Lunelli, L., Serra, M. D., Froelich, C. J., Gilbert, R. J. C., and Anderluh, G. (2011) Perforin activity at

membranes leads to invaginations and vesicle formation. *Proceedings of the National Academy of Sciences of the United States of America 108*, 21016-21021.

(76) Solon, J., Gareil, O., Bassereau, P., and Gaudin, Y. (2005) Membrane deformations induced by the matrix protein of vesicular stomatitis virus in a minimal system. *Journal of General Virology 86*, 3357-3363.

(77) Lamaziere, A., Burlina, F., Wolf, C., Chassaing, G., Trugnan, G., and Ayala-Sanmartin, J. (2007) Non-Metabolic Membrane Tubulation and Permeability Induced by Bioactive Peptides. *Plos One 2*, e201.

(78) Sandre, O., Moreaux, L., and Brochard-Wyart, F. (1999) Dynamics of transient pores in stretched vesicles. *Proceedings of the National Academy of Sciences of the United States of America 96*, 10591-10596.

(79) Jaalouk, D. E., and Lammerding, J. (2009) Mechanotransduction gone awry. *Nature Reviews Molecular Cell Biology 10*, 63-73.

(80) Gerhold, K. A., and Schwartz, M. A. (2016) Ion Channels in Endothelial Responses to Fluid Shear Stress. *Physiology 31*, 359-369.

(81) Yasuda, N., Miura, S. I., Akazawa, H., Tanaka, T., Qin, Y., Kiya, Y., Imaizumi, S., Fujino, M., Ito, K., Zou, Y., Fukuhara, S., Kunimoto, S., Fukuzaki, K., Sato, T., Ge, J. B., Mochizuki, N., Nakaya, H., Saku, K., and Komuro, I. (2008) Conformational switch of angiotensin II type 1 receptor underlying mechanical stress-induced activation. *Embo Reports 9*, 179-186.

(82) Soubias, O., Teague, W. E., Hines, K. G., and Gawrisch, K. (2014) The role of membrane curvature elastic stress for function of rhodopsin-like G protein-coupled receptors. *Biochimie 107*, 28-32.

(83) Zhang, Y. L., Frangos, J. A., and Chachisvilis, M. (2009) Mechanical stimulus alters conformation of type 1 parathyroid hormone receptor in bone cells. *American Journal of Physiology-Cell Physiology 296*, C1391-C1399.

(84) Chen, K. D., Li, Y. S., Kim, M., Li, S., Yuan, S., Chien, S., and Shyy, J. Y. J. (1999) Mechanotransduction in response to shear stress - Roles of receptor tyrosine kinases, integrins, and Shc. *Journal of Biological Chemistry 274*, 18393-18400.

(85) Hoffman, B. D., Grashoff, C., and Schwartz, M. A. (2011) Dynamic molecular processes mediate cellular mechanotransduction. *Nature 475*, 316-323.

(86) De Pascalis, C., and Etienne-Manneville, S. (2017) Single and collective cell migration: the mechanics of adhesions. *Molecular Biology of the Cell 28*, 1833-1846.

(87) Yamamoto, K., and Ando, J. (2018) Emerging Role of Plasma Membranes in Vascular Endothelial Mechanosensing. *Circulation Journal 82*, 2691-2698.

(88) Halder, G., Dupont, S., and Piccolo, S. (2012) Transduction of mechanical and cytoskeletal cues by YAP and TAZ. *Nature Reviews Molecular Cell Biology 13*, 591-600.

(89) Low, B. C., Pan, C. Q., Shivashankar, G. V., Bershadsky, A., Sudol, M., and Sheetz, M. (2014) YAP/TAZ as mechanosensors and mechanotransducers in regulating organ size and tumor growth. *Febs Letters 588*, 2663-2670.

(90) Mellouli, S., Monterroso, B., Vutukuri, H. R., te Brinke, E., Chokkalingam, V., Rivas, G., and Huck, W. T. S. (2013) Self-organization of the bacterial cell-division protein FtsZ in confined environments. *Soft Matter 9*, 10493-10500.

(91) Wei, Y., Mayoral-Delgado, I., Stewart, N. A., and Dymond, M. K. (2019) Macromolecular crowding and membrane binding proteins: The case of phospholipase A(1). *Chemistry and Physics of Lipids 218*, 91-102.